Available online at www.sciencedirect.com
ScienceDirect
Journal of the European Ceramic Society 27 (2007) 4813–4820
www.elsevier.com/locate/jeurceramsoc

Microstructure-induced thermal stresses in pyrolytic carbon matrices at temperatures up to 2900 °C

R. Piat [a,*], Y. Lapusta [b], T. Böhlke [a], M. Guellali [c], B. Reznik [d], D. Gerthsen [d], Tengfei Chen [d,e], R. Oberacker [c], M.J. Hoffmann [c]

[a] *Institute of Engineering Mechanics, University of Karlsruhe, Kaiserstr 12, 76128 Karlsruhe, Germany*
[b] *French Institute of Advanced Mechanics, IFMA-LAMI, Campus de Clermont-Ferrand les Cezeaux, BP 265-63175 Aubiere Cedex, France*
[c] *Institute of Ceramics in Mechanical Engineering, University of Karlsruhe, Haid-und-Neu-Str. 7, D-76131 Karlsruhe, Germany*
[d] *Laboratory for Electron Microscopy, University of Karlsruhe, D-76128 Karlsruhe, Germany*
[e] *Changsha University of Science and Technology, 410076 Hunan, China*

Received 25 November 2006; received in revised form 16 March 2007; accepted 25 March 2007
Available online 21 May 2007

Abstract

Carbon/carbon composites produced by chemical vapor infiltration consist of carbon fibers embedded in a pyrolytic carbon matrix with a cylindrically layered structure at the microscale. Each coating layer has a different texture and different mechanical properties that depend on temperature. Stress distributions in such carbon matrices subjected to thermal loading and their possible failure scenarios are analyzed. A two-scale numerical model is developed. At the nanoscale, material properties of each layer are determined using a methodology based on the Eshelby's theory for continuously distributed inclusions. The resulting material parameters for each layer are then used in the finite element modeling at the microscale. Calculations are conducted for composites with different matrix structures for several cases of thermal loading. Calculated stress distributions show zones of maximal stress concentration and provide information on possible failure regions which correspond well with experimentally identified failure regions.

Keywords: Chemical vapor infiltration; Composites, Failure analysis; Thermal properties; Carbon

1. Introduction

Carbon/carbon composites fabricated by chemical vapor infiltration (CVI) of carbon fiber felts have a complex hierarchical microstructure.[1,2] They consist of carbon fibers embedded in a pyrolytic carbon matrix. This matrix around the fibers has a cylindrically layered structure with each layer having different mechanical properties in the axial, radial and circumferential directions. These layers correspond to different dominating orientation distributions of basal planes (texture) in pyrolytic carbon (see Fig. 1). Using classification proposed in Ref. [3] the different textures of pyrolytic carbon matrices can be defined as isotropic (ISO), low-textured (LT), medium-textured (MT) and high-textured (HT). The texture of the pyrolytic carbon can be strongly influenced by the chemical vapor infiltration parameters (temperature, pressure, residence time, ratio between surface area and free volume) and by the post-heat treatment conditions (temperature, dwell time).

To fabricate carbon/carbon composites for industrial applications, heat treatments above 2000 °C are applied commonly after densification to a suitable density.[4] Our investigations of the influence of heat treatments on the microstructure and properties of carbon/carbon composites show that extensive cracks appear in the medium-textured pyrolytic matrix after heat treatment. Similar observations are reported in Ref. [5]. Cracks induced during the heat treatment may reduce dramatically the performance of the composite. In this work we analyze the influence of heat treatments on stress distributions and crack initiation in a medium-textured and high-textured pyrolytic carbon matrix produced by chemical vapor infiltration of carbon fiber felts. After presenting the experimental procedure, a two-scale modeling of stress distributions in these composites under high temperature is presented. Note that stress fields for fiber composites under

* Corresponding author. Tel.: +49 721 608 8853; fax: +49 721 608 4187.
E-mail address: piat@itm.uni-karlsruhe.de (R. Piat).

0955-2219/$ – see front matter © 2007 Elsevier Ltd. All rights reserved.
doi:10.1016/j.jeurceramsoc.2007.03.023

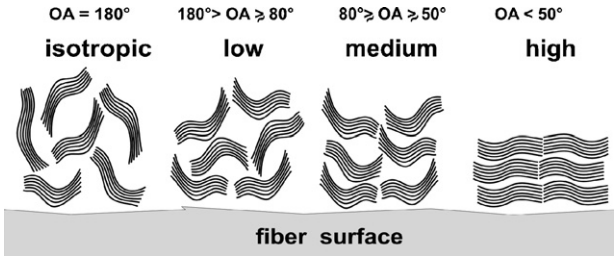

Fig. 1. Schematic presentation of the different dominating orientation distributions of basal planes in different layer textures.

thermomechanical loading and some related problems were analyzed, among others, in Refs. [6–9]. This was done mostly at the microscale with the use of concentric cylinder models. Here, the analysis focuses on both the micrometer and the nanometer scales. Stress distributions in and around carbon fibers for different textures of the surrounding pyrolytic carbon layers are studied for different cases of thermal loading.

2. Experimental procedure and observations

Carbon fiber felts (CCKF 1001, Sintec, Germany), made of randomly oriented chopped carbon fibers as shown in the SEM micrograph Fig. 2a, are used as preform for the infiltration. The fiber volume content is about 12%. The felts were infiltrated by means of an isothermal chemical vapor infiltration (I-CVI) process at different infiltration parameters (Fig. 2b) to obtain resulting material (Fig. 2c). The infiltration was carried out at the Institute for Chemical Technology of the Karlsruhe University (group of Prof. Hüttinger) in a vertical gap reactor shown in Fig. 2 using pure methane as precursor gas. Details on the infiltration procedure are given in Ref. [10].

Polarized light microscopy (PLM) investigations on polished cross-sections presented in Fig. 2 shows that the pyrolytic carbon matrix around the fibers has the shape of cylindrical layers at the micrometer scale. These have different widths and optical anisotropy.[1,11] An increased optical anisotropy correlates with an increased degree of texture. The textures of the deposited pyrocarbons were determined using an OLYMPUS AX70 microscope equipped with a polarizor and rotating analyzer according to their optical activity and value of the extinction angle A_e as described in Ref. [12]. The corresponding pyrocarbon optical textures with a progressive anisotropy degree are defined as isotropic (ISO, $A_e < 4°$), low-textured or dark laminar (LT or DL, $4° \leq A_e < 12°$), medium-textured or smooth laminar (MT or SL, $12° \leq A_e < 18°$), and high-textured or rough laminar (HT or RL, $A_e \geq 18°$).[12,3] These textures can also be characterized by selected area electron diffraction (SAED)[13] on sub-μm scale. The SAED investigations were carried out on transversal sections perpendicular to the fiber orientation using a 120 keV Zeiss EM 912 Omega transmission electron microscope equipped with an electron-energy filter integrated into the projection lens system. The extracted orientation angles (OA) are: $80° < OA < 180°$, $50° \leq OA < 80°$ and $OA < 50°$ for LT-, MT– and HT–carbon, respectively.

We study here materials with two different pyrolytic carbon matrix types, HT and MT. Their PLM micrographs are presented in Fig. 3. The HT-material (Fig. 3a) has a predominantly high-textured pyrolytic carbon matrix, the MT-material (Fig. 3b) has a mainly medium-textured pyrolytic carbon matrix.

These materials were treated in a vertical high temperature furnace (Thermal Technology Inc.) with a graphite-heating element for 2 h under a very pure helium atmosphere. Due to the high thermal radiation flux, a uniform temperature can be supposed for the entire sample. Fig. 4 shows schematically the realized experimental setup. In the experiment, two thermal regimes have been applied: heating up to 2200 °C and heating up to 2900 °C. The process of the thermal loading is the following. First the temperature is raised up to 1500 °C (60 min) in a power control regime. Then the thermal loading continued up to 2200 °C with a rate of 10 °C/min. Up to 2500 °C,

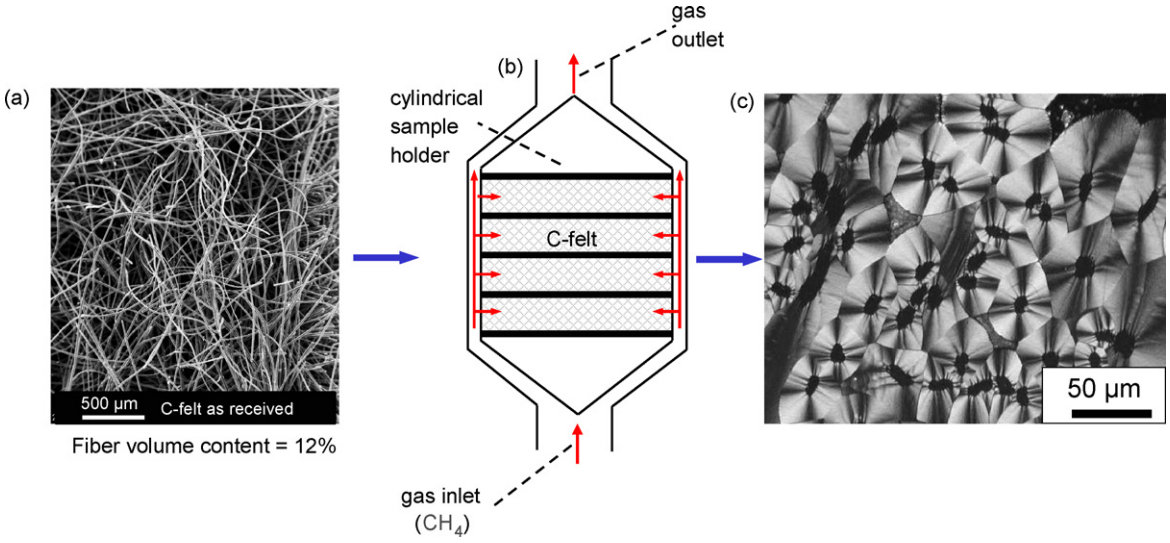

Fig. 2. Experimental setup and microstructure of the investigated materials: (a) SEM image of carbon fiber-felt preform; (b) scheme of CVI reactor; (c) PLM image of the resulting material.

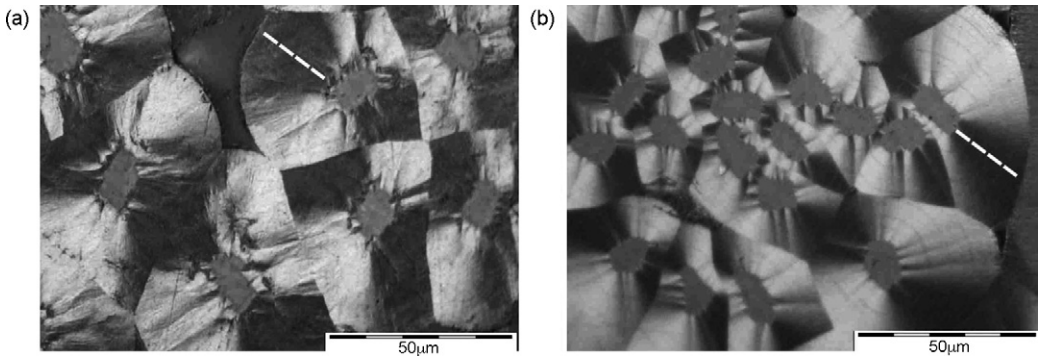

Fig. 3. Microstructure of the initial (as infiltrated) materials: (a) material with HT–pyrolytic carbon matrix; (b) material with MT–pyrolytic carbon matrix. White dashed lines mark the tracks of SAED scans.

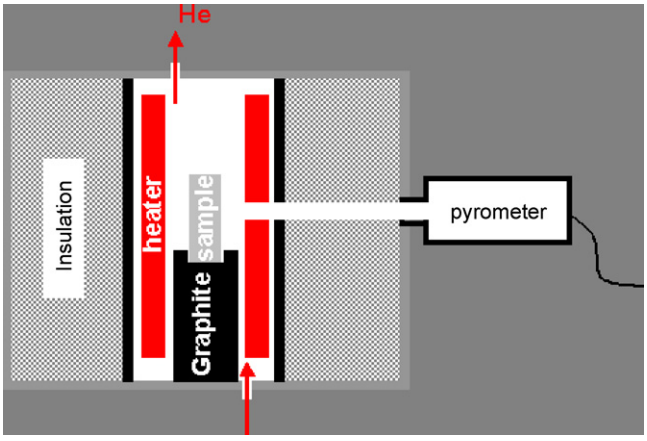

Fig. 4. Experimental setup for the heat treatments.

a rate of 5 °C/min is used. In the intervals 2500–2700 °C and 2700–2900 °C, a rate of 3 °C/min and 2 °C/min is applied, respectively. For both regimes, after reaching the maximal temperature, the furnace was turned off and cooling down was running in closed reactor.

The samples were studied by means of selected area electron diffraction before and after the heat treatment. Microscopic specimens consisting of fibers surrounded by pyrolytic carbon matrices were extracted from each material. SAED investigations were performed with a selected area aperture allowing the analysis of a specimen area of about 550 nm in diameter. Values of OA as a function of the distance to fiber surface were obtained. These values are used in the modeling. Observations were conducted starting with the aperture located close to the fiber surface and then moving in the radial direction to the coating boundary with a fixed step distance.

3. Material characterization

PLM images of the microstructure of two studied materials at room temperature are presented in Fig. 3. The OA measurement results in the matrix for both materials are presented in Fig. 5. In this figure, OA as a function of the distance to the fiber surface for the (a) HT–pyrolytic carbon matrix and (b) MT–pyrolytic carbon matrix are given.

On each graph, the values are plotted for the same origin material whose OA corresponds to the curve with notation RT (room temperature, without thermal treatment). The curves with notation 2200 °C and 2900 °C correspond to the OA measurement at RT on the samples which were heated to these temperatures and then cooled off to the RT. The analysis of these graphs shows that the HT pyrolytic carbon has changed significantly its microstructure after thermal loading to 2200 °C. After thermal loading to 2900 °C, the material is graphitized. In contrast, in the MT pyrolytic carbon, the OA changes induced by thermal loading are less significant. The obtained values of OA are then used for modeling the material properties.

4. Modeling

A two-scale model making it possible to predict thermal stresses which account for the microstructure changes during

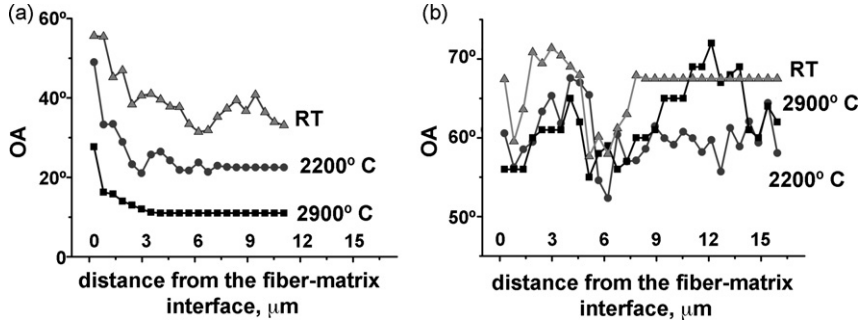

Fig. 5. Results of OA measurement (in degrees): (a) material with mainly HT-pyrolytic carbon matrix; (b) material with mainly MT–pyrolytic carbon matrix.

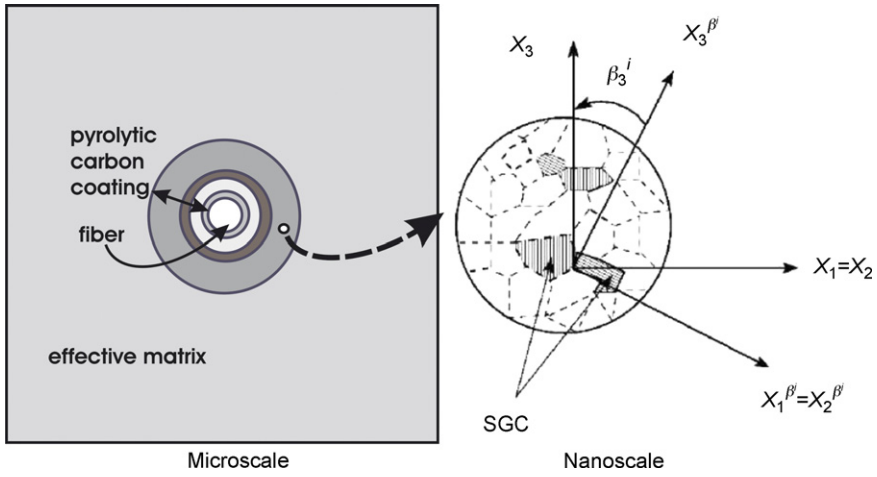

Fig. 6. Two-scale model: geometry of the FEM model at the microscale and RVE at the nanoscale consisting of coherent domains, modeled as single graphite crystals (SGCs).

heating up to 2900 °C was developed (Fig. 6). The matrix material at the nanoscale is described through distributed coherent carbon domains. At the microscale, the material is presented by a carbon fiber surrounded by several pyrolytic carbon layers. This system is embedded in an isotropic matrix with the effective material properties of the composite.

4.1. Nanoscale

The representative volume element (RVE) selection is based on considering the ratio between the diameters of the analyzed area, i.e. the diameter of SAED aperture (characteristic length L) with respect to a sufficiently small average size of the coherent domains (characteristic length l). The size of the coherent domains can be extracted from high-resolution (HR) TEM images.[15] In our case, the diameter of SAED aperture is about 550 nm, i.e. a relatively large region is analyzed. The maximal value of the coherent domain size l is taken equal to 15 nm. The corresponding coefficient $k = l/L$ is about 2.7×10^{-2}, i.e. fulfils the selection criteria of the RVE.[14]

The statistical RVE on the nanoscale is defined for each texture of pyrolytic carbon. We assume a spatial periodicity of a nanoscopic RVE as well as a local uniformity of microscopic fields within each RVE. The RVE is modeled as a polycrystal.

Each single crystal of the polycrystal may be treated as an inclusion embedded in the remaining crystals. In this case, there is complete symmetry in treating each crystal as an inclusion.[14] Therefore, the pyrolytic carbon is modeled as a system of single graphite crystals (SGC) embedded in an infinite homogeneous matrix with unknown effective (overall) elastic moduli. Each SGC is characterized by the angles $\beta^j = (\beta_1^j, \beta_2^j, \beta_3^j)$ between the transversal isotropy axis $X_j^{\beta^i}$ of the graphite crystal (in the local coordinate system of the crystal) and X_j in the global coordinate system (Fig. 6). The elasticity tensor of the material and tensor of thermal expansion were calculated using a method described in Refs. [15,16].

The same method can be used for the calculation of the heat conductivity of the graphite crystal which has the following form in the global coordinate system:

$$\lambda^{\beta^i} = Q^{\beta^i T} \lambda Q^{\beta^i}. \tag{1}$$

Here Q^β is a transformation matrix for the crystals with orientation angle β^i and λ is composed of the heat conductivity coefficients (components $\lambda_{ii} = \lambda^\perp, \lambda^{||}$) of graphite in the local coordinate system. The graphite is an orthotropic material and X_1, X_2, X_3 are its orthotropy directions. Therefore, we have $\lambda_{ij} = 0$ for $i \neq j$. Using the rule of mixtures (see, e.g.[17]), we get from Eq. (1) the averaged values of all crystal aggregates in the form:

$$\begin{aligned} \lambda^{\perp^{\beta^i}} &= \lambda^\perp \cos^2 \beta^i + \lambda^{||} \sin^2 \beta^i, \\ \lambda^{||^{\beta^i}} &= \lambda^\perp \sin^2 \beta^i + \lambda^{||} \cos^2 \beta^i. \end{aligned} \tag{2}$$

The unknown values of λ for discrete crystal distributions (with n different crystal orientations) can be calculated as:

$$\hat{\lambda} = \sum_{\beta^i}^{n} f^{\beta^i} \lambda^{\beta^i}, \tag{3}$$

where f^{β^i} is the volume fraction of crystals with orientation angle β^i. The continuous distribution of crystal orientations for each type of texture is experimentally derived as a Gaussian distribution function $f(\beta)$ with a full width at half maximum corresponding to the measured OA value. Then the effective coefficients of heat conductivity (3) in the global coordinate system can be calculated as a limit with $\Delta\beta^i = \beta^i - \beta^{i-1} \to 0$

$$\begin{aligned} \hat{\lambda}^\perp &= \lim_{\Delta\beta^i \to 0} \sum_{\beta^i} f^{\beta^i} \lambda^{\perp^{\beta^i}} = \lambda^\perp \int_\beta f(\beta) \cos^2 \beta \, \mathrm{d}\beta \\ &\quad + \lambda^{||} \int_\beta f(\beta) \sin^2 \beta \, \mathrm{d}\beta, \quad \hat{\lambda}^{||} = \lim_{\Delta\beta^i \to 0} \sum_{\beta^i} f^{\beta^i} \lambda^{||^{\beta^i}} \\ &= \lambda^\perp \int_\beta f(\beta) \sin^2 \beta \, \mathrm{d}\beta + \lambda^{||} \int_\beta f(\beta) \cos^2 \beta \, \mathrm{d}\beta. \end{aligned}$$

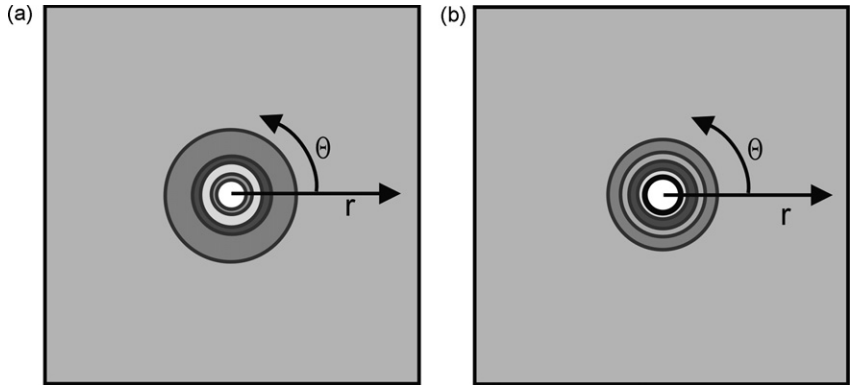

Fig. 7. Geometry used for the FEM calculation at the microscale in cylindrical coordinate system (z-axis is perpendicular to (r,θ) plane): (a) the material with mainly MT–pyrolytic carbon matrix is presented as layered structure with four sublayers; (b) the material with mainly HT–pyrolytic carbon matrix is presented as layered structure with five sublayers.

4.2. Microscale

Distributions of thermal stresses within a carbon/carbon composite are evaluated by a finite element model. The experimentally obtained values of OA (Fig. 5) are used to determine the anisotropic mechanical properties of the matrix material around the fibers as described in previous section.

The pyrolytic carbon surrounding each fiber was subdivided into several concentric layers to achieve a small variation of the orientation angle within each layer. Continuous changes of the OA within each layer were approximated through some average value which is constant within this layer. Fig. 7b and a presents microscale models for the material with mainly HT–pyrolytic carbon matrix consisting of five layers and for the material with mainly MT–pyrolytic carbon matrix consisting of four layers, respectively. The fiber and surrounding layers are embedded in an isotropic material with averaged properties of the whole composite.

5. Results and discussion

For each layer, the mechanical properties are calculated in a polar coordinate system by the nanoscale model, which are used as input for the FEM calculation at the microscale. Examples for the calculation of the mechanical and thermal properties are presented in Tables 1 and 2.

Using the developed two-scale model, the radial σ_r and tangential σ_θ stresses are then calculated for the HT–pyrolytic and MT–pyrolytic carbon matrices at different temperatures. FEM calculations are performed using Abaqus software.[18] A plane strain state and perfect bonding at the fiber–matrix interface are assumed. For each material, simulations of three temperature-loading cases were performed: thermal loading up to 1800 °C; 2200 °C and 2900 °C. Calculated stresses for both materials are presented in Figs. 8 and 9. Analyzing the results for the HT–pyrolytic and MT–pyrolytic carbon matrices for different cases of thermal loading, one can see regions with jumps (rapid

Table 1
Material parameters (in a cylindrical coordinate system (Fig. 7)) for FEM calculations: layers 2 and 3 of the HT-pyrolytic carbon coating for RT, 2200 °C and 2900 °C.

Layer	Temperature (°C)	OA	α_r (10^{-6}/°C)	$\alpha_\theta = \alpha_z$ (10^{-6}/°C)	E_r (GPa)	$E_\theta = E_z$ (GPa)	μ (GPa)	λ_r (W/cm °C)	$\lambda_\theta = \lambda_z$ (W/cm °C)
2	RT	46.05	21.56	2.65	68.41	752	105	4.2	25
	2200	31.15	23.17	1.02	43.94	881	65.73	2.1	27.1
	2900	14.9	24.5	−0.28	40	980	50	0.8	28.3
3	RT	39.16	22.26	1.94	56	828	89	3.2	26
	2200	23.77	23.9	0.28	42	886	54	1.2	27.8
	2900	11	24.5	−0.28	39	1000	45	0.7	29

Table 2
Material parameters used for FEM calculations: layers 2 and 3 of the MT–pyrolytic carbon coating for RT, 2200 °C and 2900 °C

Layer	Temperature (°C)	OA	α_r (10^{-6}/°C)	$\alpha_\theta = \alpha_z$ (10^{-6}/°C)	E_r (GPa)	$E_\theta = E_z$ (GPa)	μ (GPa)	λ_r (W/cm °C)	$\lambda_\theta = \lambda_z$ (W/cm °C)
2	RT	69.4	18.3	5.8	145	706.5	156.3	7.4	21.5
	2200	64.1	19	4.8	124.04	724.76	146.1	6.3	22.3
	2900	61	19.2	4.4	115.57	744.35	141.54	6.1	22.8
3	RT	60	19	4.3	112.26	736	139.6	6	23
	2200	58	20	4.2	105.3	743	135.4	4.9	23.5
	2900	57	21	4	104.39	744.35	134.86	5.8	23.7

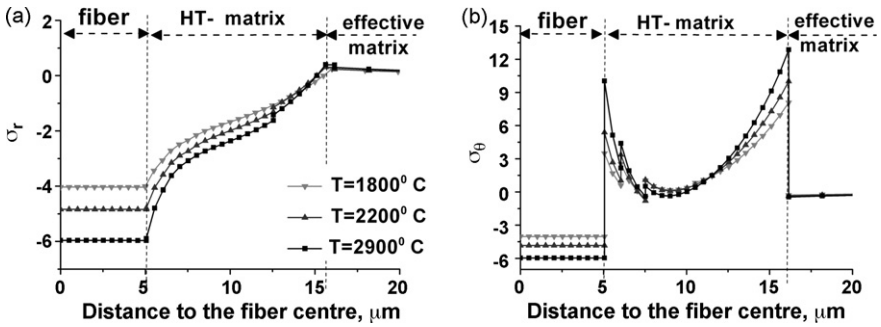

Fig. 8. Calculated (a) radial σ_r and (b) tangential σ_θ stresses for different thermal loadings for a material with HT–pyrolytic carbon matrix.

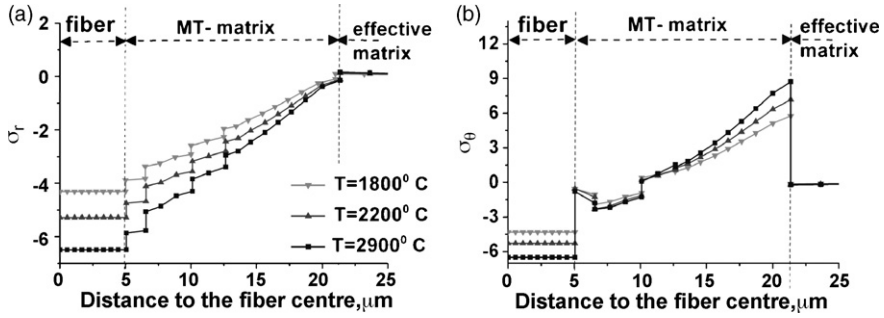

Fig. 9. Calculated (a) radial σ_r and (b) tangential σ_θ stresses for a material with MT–pyrolytic carbon matrix for different thermal loadings.

changes) of radial and tangential stresses. This is due to the assumption that the material parameters are constant within each layer.

Note that, in reality, all material properties are continuous functions of the distance to the fiber surface. In this context, the observed stress jumps simply reflect the change of material properties across the model-induced interfaces at the microscale. Depending on the stress level, local properties, microstructure geometry and critical stresses corresponding to local failure, the regions can be determined where microcracks appear first. Maximal stresses for the HT–pyrolytic and MT–pyrolytic carbon matrices are observed at the fiber–matrix interfaces. This means that microcracking is most probable in the vicinity of the fiber–matrix interfaces. Its onset will depend on the local characteristics of the HT–pyrolytic and MT–pyrolytic carbon matrices.

Light micrographs for the HT–pyrolytic and MT–pyrolytic carbon matrices are presented in Figs. 10 and 11. After thermal loading up to 2200 °C and 2900 °C, microcracking is not observed in the HT material (Figs. 10a and 11a). During thermal loading of this material, its OA values decrease almost monotonely and tend continuously to the properties of partially graphitised material (Fig. 5a). Consequently due to the lack of strong and abrupt changes of material parameters (microstructure-induced "interfaces"), there are no regions of possible microcracking, which are predefined by the microstructure or local material properties for the thermal loading until 2200 °C and 2900 °C.

On the other hand, microscopical observations of the MT–pyrolytic carbon matrices after thermal loading (Figs. 10b and 11b) detected microcracks located, as predicted by the two-scale numerical model, in the vicinity of the fiber–matrix

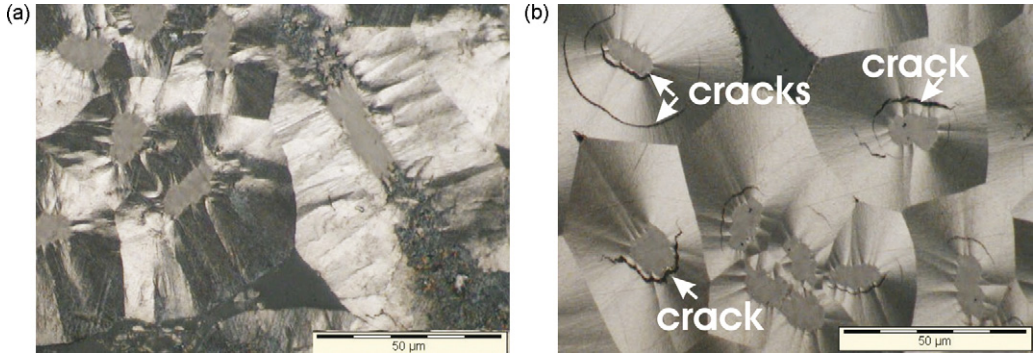

Fig. 10. Microstructure of the studied materials after thermal loading to 2200 °C: (a) material with HT-pyrolytic carbon matrix; (b) material with MT–pyrolytic carbon matrix.

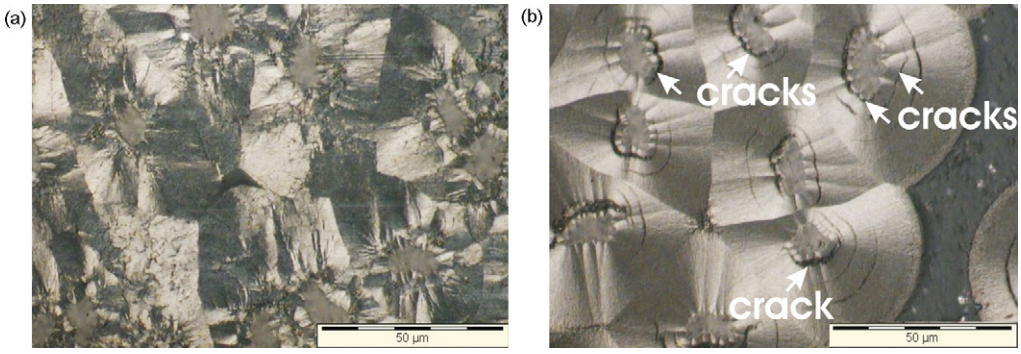

Fig. 11. Microstructure of the studied materials after thermal loading up to 2900 °C: (a) material with HT–pyrolytic carbon matrix; (b) material with MT–pyrolytic carbon matrix.

interfaces. The appearance of further matrix cracks situated at larger distances from the fiber–matrix interface (regions 2 and 3) can be explained similarly by the achieved stress levels and local microstructure in those regions. In the MT–pyrolytic carbon matrix, pronounced variations of the texture (OA-values Fig. 5b) remain after thermal loading. The onset of concentric microcracking results from the temperature-induced tangential and radial stresses due to texture variations and corresponding changes of the local material properties of the MT–pyrolytic carbon in these regions.

Due to the experimental and numerical results, one of the possible sequences of local failure is the following one. First microcracks are initiated not far from the fiber–matrix interfaces. Following this initial microcracking and the corresponding sequence of stress redistributions around the fibers, concentric microcracks appear at larger distance from the fiber–matrix interface (in the second and third regions). Note that thermal loading of the MT–pyrolytic carbon matrix up to 2900 °C (Fig. 11b) resulted in a somewhat more intensive cracking than thermal loading up to 2200 °C (Fig. 10b). This can be evidently explained by higher levels of temperature-induced stresses and microstructure changes during and after thermal loading up to 2900 °C as compared to the thermal loading up to 2200 °C.

6. Conclusions

An experimental and numerical study of carbon/carbon composites with predominantly HT– and MT–pyrolytic carbon matrices subjected to three cases of thermal loading (up to 1800 °C, 2200 °C and 2900 °C) was performed. For both materials, the texture (OA values) was characterized on a sub-μm scale by selected area electron diffraction in a transmission electron microscope as a function of the distance to fiber interface before and after thermal loading. For the material with the HT matrix, significant changes of the texture during thermal loading were observed, which leads to a monotone behavior of the texture as a function of the distance to the fiber interface. For the MT material, the variations of the texture within the matrix remain insignificant after thermal loading.

A two-scale model of the temperature-induced stresses in carbon/carbon composites was developed to predict stresses resulting from heating. From nanoscale modeling, the local material characteristics around fibers are determined. At the microscale, a FEM modeling is used. In this model, for simplicity, a perfect bonding at the fiber–matrix interface is assumed and the continuous changes of the OA were approximated by step functions. This resulted in material properties around fibers being also step functions of the distance to the fiber interface. This permits the application of a model in which the studied material was approximated by different layers of pyrolytic carbon. The material properties in each layer are constant. The developed two-scale model was used to predict thermal stress distributions in the HT– and MT–pyrolytic carbon matrices around the carbon fibers resulting from thermal loading up to 1800 °C, 2200 °C and 2900 °C. The calculation results show that microcrack initiation is most probable in the vicinity of the fiber–matrix interfaces and will depend on the local characteristics of pyrolytic carbon matrices near the interfaces and on the interface properties. No microcracking was observed experimentally in the HT–pyrolytic carbon matrix, which can be explained by the homogeneous matrix texture after thermal loading. On the contrary, concentric microcracks were experimentally observed in the MT–pyrolytic carbon matrix after thermal loading up to 2200 and 2900 °C. On the basis of the numerical results, this can be explained by the achieved stress levels and local microstructure which is characterized by pronounced texture variations even after high-temperature treatment.

Acknowledgement

The financial support by the German Research Foundation (DFG) within the framework of the Research Excellence Center (SFB) 551 “Carbon from the gas phase: elementary reactions, structures and materials” is gratefully appreciated.

References

1. Reznik, B., Gerthsen, D. and Hüttinger, K. J., Micro- and nanostructure of the carbon matrix of infiltrated carbon fiber felts. *Carbon*, 2001, **39**(2), 215–229.
2. Piat, R. and Schnack, E., Hierarchical material modeling of carbon/carbon composites. *Carbon*, 2003, **41**(11), 2121–2129.
3. Reznik, B. and Hüttinger, K. J., On the therminology for pyrolytic carbon. *Carbon*, 2002, **40**, 621–624.

4. Savage, G., *Carbon-Carbon Composites*. Chapman & Hall, London, 1993.
5. Granoff, B., Pierson, H. O. and Schuster, D. M., The effect of chemical vapor deposition conditions on the properties of carbon-carbon composites. *Carbon*, 1973, **11**, 177–187.
6. Mikata, Y. and Taya, M., Stress field in a coated continuous fibrous composite subjected to thermomechanical loading. *Journal of Composite Materials*, 1985, **19**, 554–578.
7. Stucu, M., A recursive concentric cylinder model for composites containing coated fibers. *International Journal of Solids and Structures*, 1992, **29**(2), 197–213.
8. You, L., Long, S. and Rohr, L., Elastic plastic stress field in a coated continuous fibrous composite subjected to thermomechanical loading. Transactions of the ASME. *Journal of Applied Mechanics*, 1999, **66**, 750–757.
9. Babeshko, M. E. and Shevchenko, Yu. N., Axisymmetric thermoelastoplastic stress-strain state of transversely isotropic laminated shells. *International Applied Mechanics*, 2006, **42**(6), 669–676.
10. Benzinger, W. and Hüttinger, K. J., Chemistry and kinetics of chemical vapor infiltration of pyrocarbon-V: infiltration of carbon fiber felt. *Carbon*, 1999, **37**, 941–946.
11. Reznik, B. and Gerthsen, D., Microscopic study of failure mechanisms in infiltrated carbon fiber felts. *Carbon*, 2003, **41**(1), 57–69.
12. Bourrat, X., Trouvat, B., Limousin, G., Vignoles, G. and Doux, F., Pyrocarbon anisotropy as measured by electron diffraction and polarized light. *Journal of Materials Research*, 2000, **15**(1), 92–101.
13. Reznik, B., Gerthsen, D., Zhang, W. and Hüttinger, K. J., Texture changes in the matrix of an infiltrated carbon fiber felt studied by polarized light microscopy and selected area electron diffraction. *Carbon*, 2003, **41**(2), 376–380.
14. Nemat Nasser, S. and Hori, M., *Micromechanics: Overall Properties of Heterogeneous Materials*. North-Holland, Amsterdam, 1999.
15. Piat, R., Reznik, B., Schnack, E. and Gerthsen, D., Modeling the effect of microstructure on the elastic properties of pyrolytic carbon. *Carbon*, 2003, **41**(9), 1858–1861.
16. Piat, R. and Schnack, E., Modeling the effect of microstructure on the coefficients of thermal expansion of pyrolytic carbon. *Carbon*, 2003, **41**(11), 2163–2166.
17. Chawla, K. K., *Composite Materials*. Springer, New York, 1987.
18. Abaqus software, www.abaqus.com.